What happens downstream of a dam during a flush? Insight through laboratory experiments

Robin Meurice
Catholic University of Louvain

Brieuc Bosseler
Catholic University of Louvain

Sandra Soares-Frazão
Catholic University of Louvain

What happens downstream of a dam during a flush? Insight through laboratory experiments

R. Meurice, B. Bosseler, G. Noël & S. Soares-Frazão
Université catholique de Louvain, Institute of Mechanics, Materials and Civil Engineering, Louvain-la-Neuve, Belgium

ABSTRACT: Dam flushing is often seen as a convenient way to cope with reservoir sedimentation. Yet, dam flushes may severely impact the downstream reach, which has received less attention from the scientific community than its upstream counterpart, especially in the experimental field. We conducted idealised flushing experiments with varying initial deposit depths to enhance understanding of the downstream hydromorphodynamics of dam flushes. Monitoring water and bed levels, alongside concentrations, revealed distinctions between pressure and drawdown hydromorphodynamics, emphasising the influence of the upstream deposit's depth. Moreover, we propose a non-intrusive and innovative image processing approach to calibrate the explicit inversion method employed in the acoustic backscattering framework to derive concentration profiles. Although further work is required to quantify method uncertainties, our results offer a qualitative narrative of controlled dam flushes, shedding light on the downstream dynamics.

1 INTRODUCTION

While 5% to 10% of the global capacity of dam reservoirs is already occupied by deposed sediment and 0.5% to 1% is probably lost each year, dam flushing has proved to constitute a convenient way to extend the lifetime of dam reservoirs facing sedimentation (Lehner *et al.* 2011, White 2001). Under appropriate conditions, flushing may indeed prove very efficient. Yet, such an exceptional transient flow highly laden with sediment can have major impacts on the downstream reach (Kondolf *et al.* 2014). While the populations of aquatic species can be immediately severely impacted, their habitats, and river morphology more generally, can be seriously altered (Doretto *et al.* 2022, Khakzad & Elfimov 2015).

The hydromorphodynamics of flushed reservoirs has received a vast interest from researchers, from real field cases to laboratory physical models and numerical modelling (Haun & Olsen 2012, Kantoush & Schleiss 2009, Petkovšek 2023, White 2001). On the opposite, investigations about the downstream reach have been rather limited. Several field studies have mainly focused on reporting survival rates among fish or invertebrates' populations, while a few numerical simulations have tried to reproduce the hydromorphodynamics (Espa *et al.* 2015, Liu *et al.* 2004). However, very few, if any, laboratory experiments have been reported to explicitly trying to reproduce a dam flush and investigate the downstream hydromorphodynamics. The description of these processes therefore usually remains rather simple. In particular, observations of the dynamics under the water surface during the flush are lacking in the literature.

To overcome these limitations, we conducted two-dimensional idealised dam flushing experiments in a laboratory flume. Both pressure and drawdown flushing modes were reproduced. Four configurations with different upstream initial deposit depths were tested. Water levels, morphological changes, and concentrations were evaluated throughout the whole experiment.

First, the experiment will be described, including the laboratory flume, the instrumentation, and the features of the different configurations. A particular focus will be put on the novel non-intrusive calibration method used to provide concentration profiles. Then, the results obtained will be presented. The hydrographs through the outlet will be discussed, followed by the morphological changes and the concentration profiles. Finally, conclusions about this experimental campaign will be drawn.

2 METHODS

The experiments were carried out in the installations of the Laboratoire Essais Mécaniques, Structures et génie Civil (LEMSC) at UCLouvain. The experimental flume is represented in Figure 1. Water was fed to the flume through the upstream water tank, with a constant discharge $Q = 1\ l/s$. The flume was split into two parts by a dam with a single cavity standing as the outlet of the dam. This dam was located at $x = 2.14\ m$, delimiting with a porous plate (set at $x = 1.40\ m$) a reservoir filled with water and sediment stretching over $74\ cm$. The dam outlet (opening through the plate representing the dam, see Fig. 1c for dimensions), could be open in less than 0.2 s. The flume was horizontal, except for the last metre, where the slope reached $S_0 = 0.026$. Downstream of the flume, a thin crested weir set at $z = 8.5\ cm$ led the flow to a stilling basin.

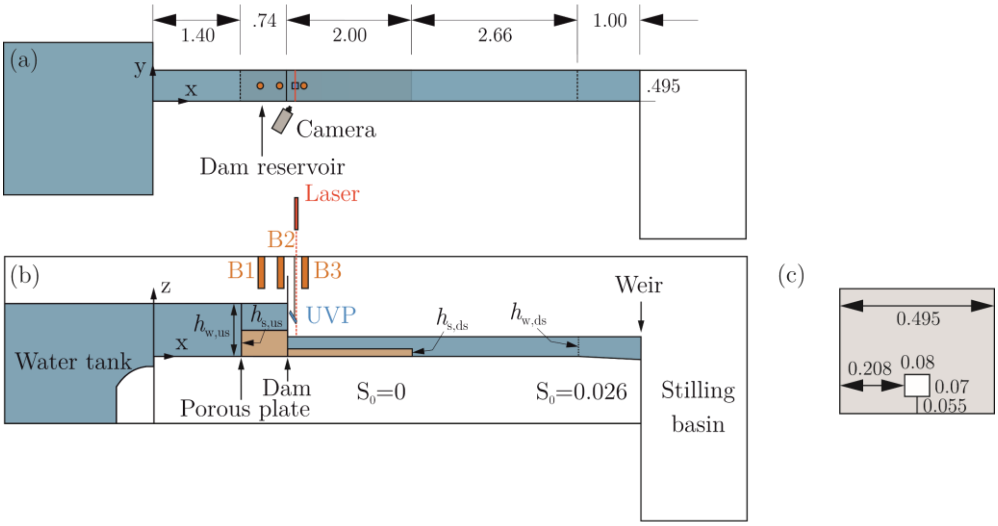

Figure 1. Experimental flume in (a) plan and (b) elevation views. Panel (c) is a sketch of the metal plate used as a dam with its outlet. The positions of the instrumentation devices are indicated in Table 1. Dimensions in metres.

Table 1. Positions of the instrumentation devices.

	Dam	B1	B2	B3	UVP	Laser
Position (m)	2.14	1.72	2.03	2.45	2.28	2.28

Four different configurations were tested during the experimental campaign. In all configurations, sand covered the first $2\ m$ downstream of the dam over $h_{s,ds} = 5.5\ cm$, i.e. the level of the invert of the outlet. The water depth up- and downstream were respectively set to $h_{w,us} = 18\ cm$ and $h_{w,ds} = 8.5\ cm$. Only the sediment depth upstream $h_{s,us}$ varied (see Table 2). Configuration C1 has no sediment upstream and is seen as a reference configuration. The sediment depth upstream $h_{s,us}$ is then respectively inferior, equal and superior to the ceiling of the outlet, i.e. $z = 12.5\ cm$.

Table 2. Sediment depth upstream of the dam in all tested configurations.

Configuration	C1	C2	C3	C4
$h_{s,us}\ (cm)$	0	9	12.5	16

A single sediment mixture was used for the different configurations. The saturated density was equal to $\rho_s = 2640\ kg/m^3$. The grain size distribution can be considered as lognormal (Fig. 2), with a granulometric dispersion $\sigma_d = \sqrt{(d_{84}/d_{16})} = 1.56$ and a median grain diameter $d_{50} = 0.359\ mm$.

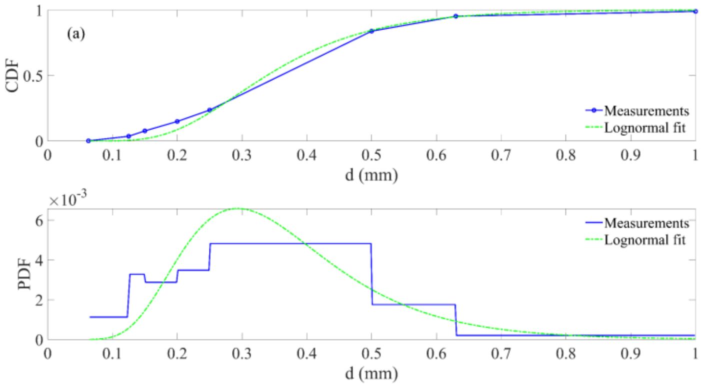

Figure 2. (a) Cumulative Density Function (CDF) and (b) Probability Density Function (PDF) of the sand used in the experiments. The CDF was interpolated with a step of 1 μm to derive the PDF. The few sieves used to establish the CDF explain the stepped appearance of the PDF. The lognormal fit uses $\mu_{log} = \log(0.5 d_{50}/\sqrt{1+\delta^2})$ and $\sigma_{log} = \sqrt{\log(\delta^2+1)}$ as distribution parameters, following Thorne & Hurther (2014), with $\delta = 0.4$.

Opening the bottom outlet starts the flush of the reservoir. During the flush, the upstream water discharge, flowing from the tank to the flume, was maintained constant ($Q = 1\ l/s$), but the discharge flowing through the outlet was larger, so that the water level in the reservoir declined. At the beginning, the water level was superior to the ceiling of the outlet ($z = 12.5\ cm$) and the flush was in pressure mode. After some time, the water level became lower than the outlet's ceiling and the flush entered the drawdown phase. Eventually, the discharge through the outlet became equal to that fed upstream and the flow became steady.

Ultrasonic Baumer sensors, labelled B1 to B3, provided a time series of point measurements of the water levels. The evolution of the topography was estimated by laser profilometry (Meurice *et al.* 2022). A linear laser sheet was projected through the water surface and the evolution of its projection onto the bed was captured by a camera located outside the transparent flume (Fig. 1a). It was therefore possible to follow the evolution of the bed during the flow along a linear profile. Moreover, photogrammetry was used to measure the final topography, once the water had been evacuated. Finally, a single-frequency 4 MHz Ultrasonic Velocity Profiler (UVP) transducer, connected to a UVP-DUO monitoring unit (Met-Flow 2011), used acoustic backscattering to estimate concentration profiles, following Pedocchi & García (2012). The UVP transducer was inclined with a counter-clockwise angle of 40° and its nozzle was set at $z = 9.5\ cm$.

Although it was developed initially for the marine environment, we used the theoretical framework defined by Thorne & Hurther (2014) to translate echo measurements made by the UVP-DUO into concentration measurements. The fundamental equation to establish these concentration profiles along the water column is as follows:

$$M(r) = \left(\frac{\psi(r)r}{k_s k_t}\right)^2 V_{rms}^2(r) e^{4r\alpha(r)} \quad (1)$$

where $M(r)$ (g/l) is the concentration at some range r (m) from the transducer's nozzle, $\psi(r)$ the near-field corrector as defined by Downing *et al.* (1995), $k_s = 2.24$ the sediment backscattering coefficient determined thanks to the general formulation of Moate & Thorne (2012) for natural particles, k_t the instrumentation coefficient (not determined here), $V_{rms}(r)$ (V) the root mean square value of the electrical tension obtained by the UVP-DUO system for the backscattered echo, and $\alpha(r) = \alpha_w + \alpha_s(r)$ the attenuation coefficient with $\alpha_w = 0.405\ Np/m$ the component due to water according to François & Garrison (1982) considering a temperature $T = 20\ °C$, and $\alpha_s(r)$ the component due to suspended particles that can be defined as:

$$\alpha_s(r) = \frac{1}{r}\int_0^r \xi M(r)dr \tag{2}$$

with $\xi = 4.77 \times 10^{-4}\ m^2/kg$ following Moate and Thorne (2012).

If the attenuation due to suspended particles $\alpha_s(r)$ cannot be neglected, Equation 1 is implicit for $\alpha_s(r)$ depends on $M(r)$. An implicit inversion algorithm was extensively used in the literature to obtain both $M(r)$ and $\alpha_s(r)$. Yet, this algorithm may diverge in some cases. Furthermore, this method requires the calibration of k_t, as proposed by Betteridge *et al*. (2008), which could not be done during this experimental campaign. Instead, we used the explicit method proposed by Lee & Hanes (1995) based on the derivation of $M(r)$ and that does not rest on k_t. Its final solution is as follows:

$$M(r) = \frac{\beta^2}{\beta_{ref}^2/M_{ref} - 4\int_{r_{ref}}^{r} \beta^2 dr} \tag{3}$$

with $\beta = V_{rms}\psi r e^{2\alpha_w r}/k_s$ and r_{ref} being a reference range, typically at the top of the ultrasonic profile. The reference concentration M_{ref} is often estimated with an intrusive sampling device like a pump (Holdaway & Thorne 1997). Considering the dimensions of the flume and the depth of the flow, direct sampling would probably have seriously influenced the flow. Instead of direct measurements, we took advantage of the LPT system to estimate M_{ref} with image processing, in a non-intrusive way. The method of Capart & Fraccarollo (2011) was adapted to determine the concentration inside a measurement volume $V_M = 311.28\ mm^3$, close to the transducer's nozzle and illuminated by the laser above the flume (Fig. 3). Considering all particles equal to d_{50}, their number *N* was evaluated so that:

$$M_{ref} = \frac{1}{V_M}\frac{4\pi}{3}\left(\frac{d_{50}}{2}\right)^3 \rho_s N \tag{4}$$

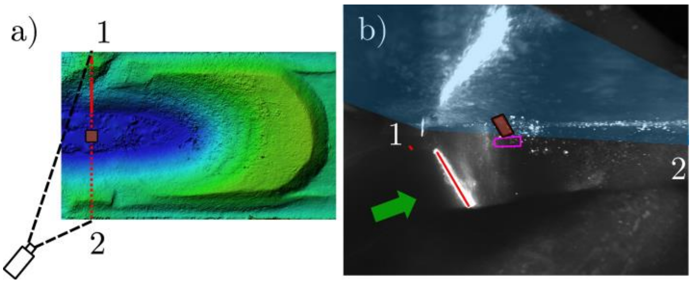

Figure 3. (a) Plan view of the final topography with respect to the camera and laser's positioning. The parts of the laser that are not visible in (b) are represented by dashed lines. The nozzle of the UVP sensor is in brown. (b) Picture captured by the camera positioned as in (a) during an experimental run. The water surface is in blue and the UVP sensor in brown. The visible parts of the laser illuminating the bed and the direction of the flow are respectively indicated in red and green. Reference points 1 and 2 correspond to those of (a). A research window (purple) delimits the measurement volume V_M.

3 RESULTS

3.1 *Hydrographs*

We computed the hydrographs through the outlet using Bernoulli's equation and water levels recorded by the Baumer sensors. In pressure mode, the water depth at the outlet was equal to $h_o = 0.07\ m$, i.e. the height of the outlet. In drawdown mode however, it depended on the Froude number. For sub- and supercritical flows, $h_o = h_{B3} = z_{B3} - 0.055\ m$ and $h_0 = h_c$ respectively, where the critical depth $h_c\ (m)$ is estimated by $h_c = 2/3\ (z_{B1} - 0.055)$, with sensor B1 being considered as far upstream (Matthew, 1963). The discharge can then be computed with Bernoulli's equation:

$$Q = \mu_O w_o h_o \sqrt{2g(z_{B2} - z_{B3})} \tag{5}$$

where $w_o = 0.08\ m$ is the width of the outlet, $g = 9.81\ m/s^2$ the gravitational acceleration, and μ_o the discharge coefficient of the outlet. Neglecting lateral head losses, $\mu_o \simeq 1$ in drawdown mode. In pressure mode however, we calibrated μ_0 to ensure the continuity of the hydrograph in C1 and obtained $\mu_0 = 0.7$. Generally, Figure 4 shows an expected decline of Q with time, as the reservoir was emptying. This is very clear for C1 and C2 that behave rather similarly. Although C3 shows the same general tendency, its hydrograph sees a strong drop between $t = 100\ s$ and $t = 150\ s$, that even reaches negative amplitudes. This is due to morphological evolutions that lead to $z_{B3} > z_{B2}$ for a while. Configuration C4 shows a similar discharge local minimum around $t = 50\ s$. Eventually, the hydrographs of all configurations converge towards the input discharge $Q = 1\ l/s$. During the experimental campaign, we observed the flow transitioned from pressure to drawdown when z_{B2} became lower than $z_{B2} = 12.9\ cm$. The transitions are indicated by the vertical dashed lines in Figure 4. It appears the deeper $h_{s,us}$, the sooner the transition, all other things being equal.

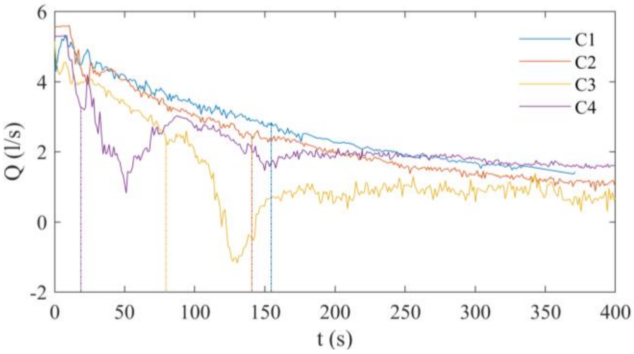

Figure 4. Hydrographs of all configurations based on Bernoulli's equation. The vertical dashed lines correspond to the pressure-drawdown transitions of each configuration.

3.2 *Morphological changes*

As evidenced by Figure 5, the different configurations show both similar and specific morphodynamical patterns that can be highlighted using three zones of the downstream sand cover. The first zone corresponds to the primary erosion pit, occurring in pressure mode and clearly visible in the final topographies of C1 and C2. In C3 and C4, that are still very dynamic in the drawdown mode, this zone receives deposition from the sediment flushed from upstream. Zone 2 is mainly constituted by deposits of the sediment eroded from zone 1 during the pressure step. The front of this zone looks to recede with $h_{s,us}$, which suggests less erosion in pressure mode in advanced configurations. Finally, zone 3 is the sand cover that is barely affected by the flushing process.

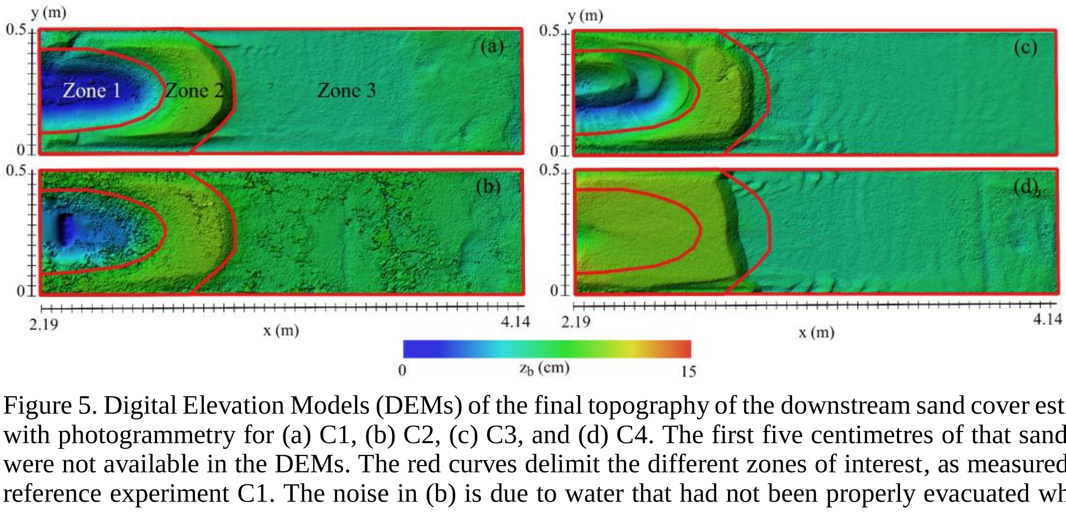

Figure 5. Digital Elevation Models (DEMs) of the final topography of the downstream sand cover estimated with photogrammetry for (a) C1, (b) C2, (c) C3, and (d) C4. The first five centimetres of that sand cover were not available in the DEMs. The red curves delimit the different zones of interest, as measured in the reference experiment C1. The noise in (b) is due to water that had not been properly evacuated when the pictures used for the DEM of C2 were captured.

These assumptions based on the final topography can be confirmed using the backscattered echo received by the UVP sensor. At the bed, the backscattered echo indeed strongly rises. If the signal has not been attenuated too much up to the bed, it is sometimes possible to estimate the bed level as a local maximum. In Figure 6a, the bed level in the transducer axis, located in zone 1 (see Fig. 3a), sees a strong reduction in C1 and C2 in the early pressure mode. In C3, soon after the transition to drawdown (see Fig. 4), the bed level starts to rise. In C4 however, we cannot see erosion from Figure 6a. To the contrary, it even suggests that there is some erosion in zone 1 in the late drawdown mode, which is contradictory to the observations. This advocates for keeping a qualitative approach when analysing morphological changes using this method.

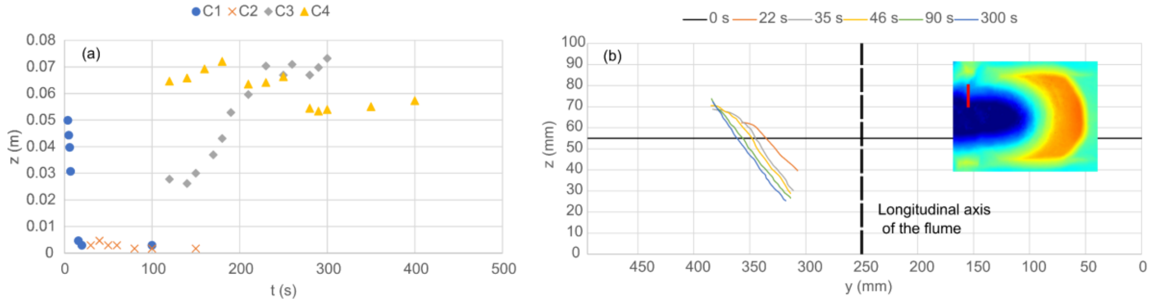

Figure 6. (a) Evolution of the bed level along the UVP transducer's axis for configurations C1 to C4. (b) Evolution of the left bank of the erosion pit in C1.

The UVP sensor is a convenient tool to evaluate the bed level in turbulent and turbid conditions but its spatial coverage is very limited. Laser profilometry was hence used to monitor the evolution of the banks of the erosion pit and its contours (Fig. 6b). As evidenced by Figure 6a, the erosion of zone 1 occurs very rapidly. Because of turbidity and turbulence, no pictures were available until $t = 22\ s$ in C1 but it appears the banks of the pit continue to stabilise until $t = 90\ s$ around a stability angle $\alpha_r \simeq 35°$ as can be seen in Figure 6b.

3.3 *Concentrations*

Using the measurement window of Figure 3b and Equation 4, M_{ref} can be obtained at the top of the UVP transducer's axis (Fig. 7a). As expected, M_{ref} increases with $h_{s,us}$. After some early oscillations, M_{ref} stabilises eventually in C1 and C2. To the contrary of C2, a surge in M_{ref} is observed at the pressure-drawdown transition in C3. Unfortunately, the laser could not be detected in C4. There is hence no estimation available for M_{ref}.

The time series of M_{ref} can be used by the explicit inversion method (Eq. 3) to establish vertical concentration profiles for C1, C2, and C3 (Fig. 7b-d). As expected, the amplitudes of the concentration profiles tend to decrease with time in C1 and C2. As suggested by Figure 6, the morphodynamics slows down very quickly in these configurations. Even though M_{ref} showed similar orders of magnitude from $t = 30\ s$ to $t = 100\ s$, the concentrations in C3 peak at a lower level than in C2 during that period. Again, this advocates for caution when analysing the UVP results. From $t = 100\ s$ to $t = 300\ s$, the bed level keeps rising in C3 (see Fig. 6a) and so do the concentration peaks.

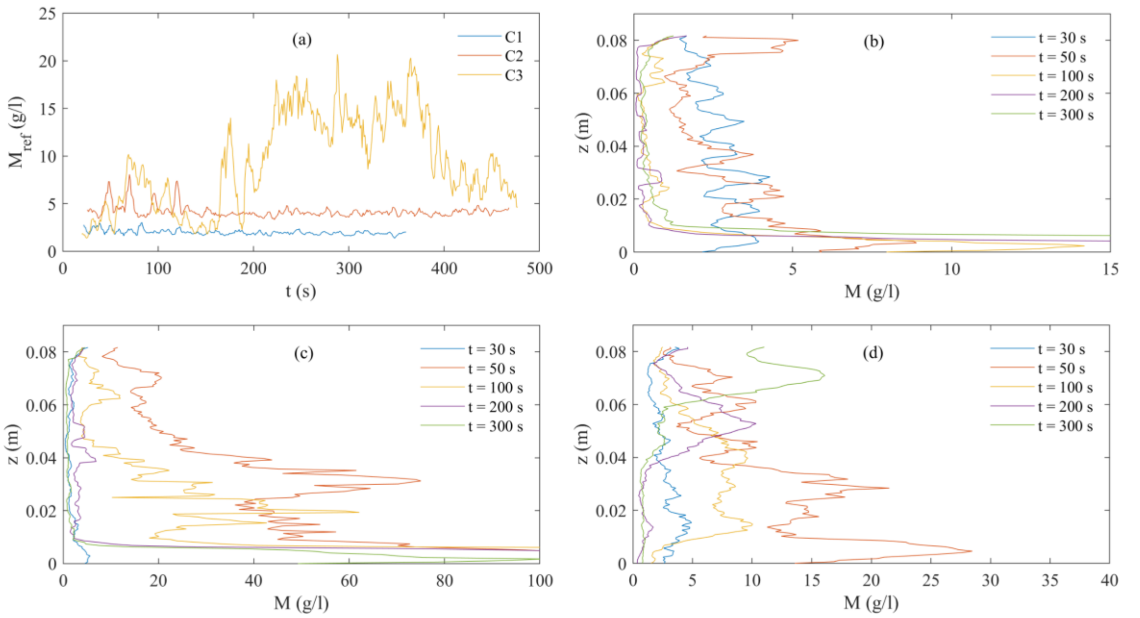

Figure 7. (a) Time series of M_{ref} for C1, C2, and C3. (b)-(d) Evolution of the vertical concentration profile for configurations C1-C3. The profiles were smoothed with a 10 channels-wide moving average window.

4 CONCLUSION

We presented the methods and results of an experimental campaign aimed at gaining a deeper understanding of the downstream hydromorphodynamics of dam flushes, which has received less focus from the scientific community compared to its upstream counterpart. The experiments consisted in flushing a reservoir containing layers of sand and water through a single outlet, which was narrower than the flume, into a downstream reach already covered with sand, extending up to the invert of the outlet. Overall, four different configurations with a varying initial upstream deposit's depth were investigated.

Ultrasonic Baumer sensors provided measurements of the water levels that were used to estimate the discharge passing through the outlet of the dam (Fig. 4). Laser profilometry, photogrammetry and acoustic backscattering were combined to monitor the downstream morphodynamics. In particular, the calibration required by the traditional explicit inversion method of acoustic backscattering was achieved following a non-intrusive approach. We indeed used the laser-camera system installed for laser profilometry and image processing to evaluate the concentration near the nozzle of the UVP used to establish concentration profiles (Fig. 7). This innovative method appears particularly appropriate in a laboratory framework, considering the shallowness of the flows and the unavoidable disturbances that would arise from using more common direct sampling methods for this calibration.

The results showed that pressure flushing leads to the excavation of an erosion pit downstream of the outlet, with deposition of the eroded sediment on the contours of the pit. This pit may then be filled during the drawdown step. Also, the deeper the initial upstream deposit, the shorter the pressure mode, leading to a limited depth for the erosion pit when the initial upstream deposit's depth is near or exceeds the ceiling of the outlet.

More work is required to refine the understanding of the hydromorphodynamical processes during pressure and drawdown flushing and to assess the impact of different factors on the downstream hydromorphodynamics. Also, the uncertainties around the applications of the UPV for acoustic backscattering in these experimental configurations must be evaluated for a proper quantitative assessment of the downstream morphodynamical changes. Yet, the complementary information delivered by the different instrumentation devices already provides more insight into the downstream hydromorphodynamical processes of a dam flush.

ACKNOWLEDGMENTS

The authors address their gratitude towards Francisco Pedocchi and Rodrigo Mosquera for their Matlab codes and help regarding the treatment of UVP data. They also thank Olivier Mariette, for assisting them to use the UVP-DUO unit as appropriately as possible, and Hervé Capart for its kind help in determining the reference concentration with image processing. Finally, they acknowledge the F.S.R.-FNRS for the financial support of Robin Meurice as an FNRS fellow.

REFERENCES

Betteridge, K. F., Thorne, P. D., & Cooke, R. D. 2008. Calibrating multi-frequency acoustic backscatter systems for studying near-bed suspended sediment transport processes. *Continental Shelf Research*, 28(2): 227-235.

Capart, H., & Fraccarollo, L. 2011. Transport layer structure in intense bed-load. *Geophysical Research Letters*, 38(20).

Doretto, A., Espa, P., Salmaso, F., Crosa, G., & Quadroni, S. 2022. Considering mesohabitat scale in ecological impact assessment of sediment flushing. *Knowledge & Management of Aquatic Ecosystems*, (423): 2.

Downing, A., Thorne, P. D., & Vincent, C. E. 1995. Backscattering from a suspension in the near field of a piston transducer. *The Journal of the Acoustical Society of America*, 97(3): 1614-1620.

Espa, P., Crosa, G., Gentili, G., Quadroni, S., & Petts, G. 2015. Downstream ecological impacts of controlled sediment flushing in an Alpine valley river: a case study. *River Research and Applications*, 31(8): 931-942.

Francois, R. E., & Garrison, G. R. 1982. Sound absorption based on ocean measurements: Part I: Pure water and magnesium sulfate contributions. *The Journal of the Acoustical Society of America*, 72(3): 896-907.

Haun, S., & Olsen, N. R. B. 2012. Three-dimensional numerical modelling of the flushing process of the Kali Gandaki hydropower reservoir. *Lakes & Reservoirs: Research & Management*, 17(1): 25-33

Holdaway, G. P., & Thorne, P. D. 1997. Determination of a fast and stable algorithm to evaluate suspended sediment parameters from high resolution acoustic backscatter systems. *7th International Conference on Electronic Engineering in Oceanography, Conference Publication No 439, Southampton, 23-25 June 1997*. London: IEE.

Kantoush, S. A., & Schleiss, A. J. 2009. Channel formation during flushing of large shallow reservoirs with different geometries. *Environmental technology*, 30(8): 855-863.

Khakzad, H., & Elfimov, V. I. 2015. Environmental reviews and case studies: a review of environmental characteristics and effects of Dez Dam flushing operation on downstream. *Environmental Practice*, 17(3): 211-232.

Kondolf, G. M., Gao, Y., Annandale, G. W., Morris, G. L., Jiang, E., Zhang, J., ... & Yang, C. T. 2014. Sustainable sediment management in reservoirs and regulated rivers: Experiences from five continents. *Earth's Future*, 2(5): 256-280.

Lehner, B., Liermann, C. R., Revenga, C., Vörösmarty, C., Fekete, B., Crouzet, P., ... & Wisser, D. 2011. High-resolution mapping of the world's reservoirs and dams for sustainable river-flow management. *Frontiers in Ecology and the Environment*, 9(9): 494-502.

Liu, J., Minami, S., Otsuki, H., Liu, B., & Ashida, K. 2004. Prediction of concerted sediment flushing. *Journal of Hydraulic Engineering*, 130(11): 1089-1096.

Matthew, G. D. 1963. On the influence of curvature, surface tension and viscosity on flow over round-crested weirs. *Proceedings of the institution of civil engineers*, 25(4): 511-524.

Met-Flow. 2011. *UVP Monitor User's Guide*. Met-Flow SA, Lausanne, Switzerland.

Meurice, R., Martínez-Aranda, S., Ebrahimi, M., García-Navarro, P., & Soares-Frazão, S. 2022. Laser Profilometry to measure the bed evolution in a dam-break flow. Journal of Hydraulic Research, 60(5): 725-737.

Moate, B. D., & Thorne, P. D. 2012. Interpreting acoustic backscatter from suspended sediments of different and mixed mineralogical composition. *Continental Shelf Research*, 46: 67-82.

Pedocchi, F., & García, M. H. 2012. Acoustic measurement of suspended sediment concentration profiles in an oscillatory boundary layer. *Continental Shelf Research*, 46: 87-95.

Petkovšek, G. 2023. Monitoring and modelling of sediment flushing: a review. *Scientific Research Communications*, 3(1).

Thorne, P. D., & Hurther, D. 2014. An overview on the use of backscattered sound for measuring suspended particle size and concentration profiles in non-cohesive inorganic sediment transport studies. *Continental Shelf Research*, 73: 97-118.

White, R. 2001. Evacuation of sediments from reservoirs. Thomas Telford.